Approximate cutting pattern optimization of frame-supported and pneumatic membrane structures

Ohsaki, Makoto; Fujiwara, Jun; Takeda, Fumiyoshi

Submitted to International Journal of Mechanics and Materials in Design

Approximate cutting pattern optimization of frame-supported and pneumatic membrane structures

Abstract

A simple iterative method is presented for cutting pattern optimization of frame-supported and pneumatic membrane structures for minimizing the variation of stresses from the target values. The plane cutting sheet is generated by minimizing the error from the shape obtained by reducing the target stress from the desired curved shape of surface. The equilibrium shape is obtained using an energy approach to minimize of total strain energy under forced deformation at the boundary nodes. The external work done by the pressure is also incorporated for analysis of pneumatic membrane structures. An approximate method is also proposed to derive a discretized form for analysis of an Ethylene TetraFluoroEthylene (ETFE) film, where elasto-plastic behavior under monotonic loading condition is modeled as a nonlinear elastic material under monotonic loading condition. The proposed method is applied to examples of a frame-supported PolyVinyl Chloride (PVC) membrane structure and an air pressured square ETFE film.

Keywords: Membrane structure, cutting pattern optimization, energy minimization, ETFE, pneumatic membrane

1. Introduction

In the field of civil and architectural engineering, curved surface structures, which are formed with pre-tensioned coated fabrics or synthetic resin films, are widely used for lightweight and long-span roofs or facades of stadiums, gymnasium and so on (Adriaessens *et al*., 2014). This kind of structure called membrane structure is also used for solar panels in space (Morozov and Lopatin, 2012). In the first step of designing process of a membrane structure, a target surface of self-equilibrium is found under given distribution of pre-tensioning stresses and boundary conditions, where in most of cases the target stress distribution is assumed to be uniform tension. Since coated fabrics and resin films are fabricated as planar sheets, the target surface is realized by connecting planar cutting sheets and clamping their edges to boundary structures such as steel frames and cables. However, curved surfaces are not generally developable to a plane, there must be some errors between the target stress distribution and the stresses of installed membrane structure.

In the process of designing a cutting pattern of plane membrane sheet, it is important to achieve a moderately uniform stress distribution to prevent fracture and slackening. Therefore, the shape of membrane sheet may be optimized in a similar manner as shape optimization of structures (Daxini and Prajapati, 2019). Although there are many methods for cutting pattern optimization, most of the methods require carrying out finite element analysis many times (Bletzinger *el al*., 2005). Ohsaki and Fujiwara (2003), Ohsaki and Uetani (2000) and Uetani *et al*. (2001) proposed a method for inversely generating the shape of cutting pattern by removing the stresses from the self-equilibrium shape. Kim and Lee (2002) presented an approximate method for a membrane divided into many strips. Punurai *et al*. (2012) used genetic algorithm for cutting pattern optimization. Philipp *et al*. (2012) proposed an updated reference strategy for form-finding of membrane structures supported by bending-active members. Extensive researches have also been carried out for surface flattening in the field of computer aided design (Wang et al., 2002; Azariadis and Aspagathos, 2001). Luo *et al*. (2017) proposed a topology optimization method for plane membrane structures to prevent wrinkling by optimizing the shapes of boundary and holes. Xing *et al*. (2018) optimized the shape of supports to suppress wrinkling of membranes subjected to large deformation.

The woven fabric membrane material has orthotropic property (Hu *et al*., 2017; Pargana *et al*., 2007). Although various sophisticated models are presented for orthotropic materials (Wang et al., 2016), properties of membrane fabrics are often simplified to isotropic or orthotropic linear elastic materials. Therefore, the equilibrium shape analysis for specified cutting pattern can be formulated as a forced displacement analysis problem, which can be solved by geometrically nonlinear analysis (Coelho *et al*., 2014a; Gosling and Lewis, 1996), dynamic relaxation method (Barnes, 1988), or minimization of the total strain energy (Mosler, 2008; Bouzidi and Le Van, 2004). However, there exists difficulty for form-finding and equilibrium shape analysis of pneumatic membrane structures that are formed and strengthened by applying air pressure (Coelho et al., 2014a; Bown and Wakefield, 2015). Bouzidi and Le Van (2004) proposed an energy minimization method for analysis of pneumatic membrane structures supported by rigid boundary incorporating a pressure potential function. However, Ethylene TetraFluoroEthylene (ETFE) film, which is often used for pneumatic membrane structures, has an elasto-plastic property; therefore, it is difficult to optimize the shape of the surface using a gradient-based optimization algorithm. Dinh *et al*. (2015) proposed an elasto-plastic material model for equilibrium shape analysis, which is applied to shape optimization of membrane with boundary cables (Dinh *et al*., 2016). To alleviate large computational cost for forced-displacement analysis, it is possible to model an elasto-plastic material by a nonlinear elastic material (Zhao *et al*., 2019).

In this paper, we present a simple iterative method for approximate cutting pattern optimization of membrane structures for minimizing the variation of stresses from the target value.

The plane cutting sheet is generated by minimizing the error from the shape obtained by reducing the stress from the desired curved shape, which is discretized into triangular finite elements. The equilibrium shape corresponding to the specified cutting pattern is obtained by solving an energy minimization problem corresponding to the forced-displacement analysis problem. The external work done by the air pressure is also incorporated for analysis of pneumatic membrane structures. The material property of ETFE film is modeled as a nonlinear elastic material assuming monotonic loading condition. It is demonstrated in the numerical examples that almost uniform stress distribution is achieved for a frame-supported PolyVinyl Chloride (PVC) membrane structure and an air-pressured square ETFE film within less than 20 analysis steps.

2. Energy minimization for equilibrium shape analysis

Self-equilibrium shape of a frame-supported membrane structure is generated by connecting plane cutting sheets to the boundary. This process is regarded as a forced deformation analysis problem, which can be solved by minimizing an energy function. In this section, we briefly present the formulation of strain energy minimization, and extend it to pneumatic membrane structures (Ohsaki *et al*., 2017).

2.1 Strain energy minimization for frame-supported membrane

Consider a curved membrane structure discretized into three-node triangular membrane finite elements with constant stress in plane stress state (Bathe 1996). The material property is assumed to be linear orthotropic elastic. Let E_x and E_y denote the elastic moduli in the two principal axes $(x_\mathrm{p}, y_\mathrm{p})$ of the material. The shear modulus is denoted by G. The following notations are used:

$$\beta = \frac{E_x}{E_y}, \quad \kappa = \frac{G}{E_y} \tag{1}$$

Then the constitutive matrix $\mathbf{D} \in \mathbb{R}^{3\times 3}$ defining the orthotropic elastic material property of the membrane is given as follows using the Poisson's ratio v_{xy}:

$$\mathbf{D} = \frac{E_y}{1-\beta v_{xy}^2}\begin{bmatrix} \beta & \beta v_{xy} & 0 \\ \beta v_{xy} & 1 & 0 \\ 0 & 0 & \kappa(1-\beta v_{xy}^2) \end{bmatrix} \tag{2}$$

Note that Poisson's ratio v_{yx} may be obtained from $v_{yx} = v_{xy} E_x / E_y$. In the following, stress is evaluated as the force per unit length of the section in accordance with the conventional formulation in thin shell theory. The vectors of inplane stress and strain with respect to the principal material coordinates of element k are denoted by $\boldsymbol{\sigma}_k = (\sigma_{kx}, \sigma_{ky}, \tau_k)^T$ and $\boldsymbol{\varepsilon}_k = (\varepsilon_{kx}, \varepsilon_{ky}, \gamma_k)^T$, respectively, where σ_{kx} and σ_{ky} are the stresses in the directions of x_p and y_p; ε_{kx} and ε_{ky} are the strains in the directions of x_p and y_p; τ_k is the shear stress; and γ_k is the shear strain. The stress-strain relation of the kth element is written as

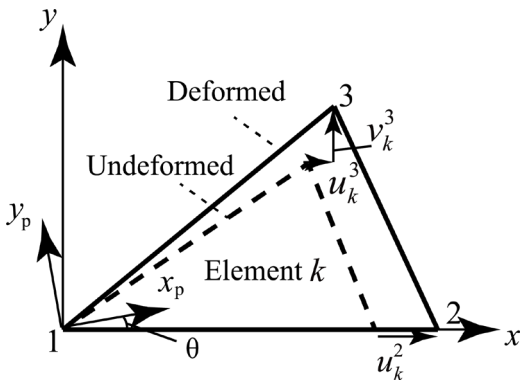

Figure 1: Local coordinates, node numbers, principal coordinates, and deformation of triangular element k.

$$\boldsymbol{\sigma}_k = \mathbf{D}\boldsymbol{\varepsilon}_k \tag{3}$$

Figure 1 defines the local (x,y)-coordinates and relative displacements from undeformed state to deformed state of element k consisting of nodes 1, 2, and 3. The displacements are fixed in x- and y-directions at node 1, and fixed in y-direction at node 2 to constrain rigid-body displacement and rotation. Let u_k^i and v_k^i denote the displacements of node i of element k, which are combined to a vector $\mathbf{u}_k = (u_k^2, u_k^3, v_k^3)^T$. The relation between the strains with respect to the principal material coordinates $(x_\mathrm{p}, y_\mathrm{p})$ and the displacements in local coordinates (x, y) is written using a strain-displacement relation matrix $\mathbf{C} \in \mathbb{R}^{3\times 3}$ and the rotation matrix $\mathbf{R} \in \mathbb{R}^{3\times 3}$ from the local coordinate systems to the directions of principal material axes as

$$\boldsymbol{\varepsilon}_k = \mathbf{R}\mathbf{C}\mathbf{u}_k \tag{4}$$

See a textbook, e.g., Bathe (1996), of finite element analysis for details.

The vector consisting of the global (X,Y,Z) -coordinates of the nodes on the surface is denoted by $\mathbf{X} \in \mathbb{R}^{n_\mathrm{d}}$, where n_d is the number of variable components of nodal coordinates after removing the specified components of the nodes along the boundary. In the process of finding the equilibrium shape using forced displacement analysis, the local displacements $\mathbf{u}_k$ are obtained by rotating the global coordinates $\mathbf{X}$ to the local coordinates, and the strain energy $S(\mathbf{X})$ of the membrane is regarded as a function of $\mathbf{X}$ as

$$S(\mathbf{X}) = \frac{1}{2}\sum_{k=1}^{m} A_k \boldsymbol{\varepsilon}_k(\mathbf{X})^T \mathbf{D}\boldsymbol{\varepsilon}_k(\mathbf{X}) \tag{5}$$

where m is the number of elements, and $A_k(\mathbf{X})$ is the area of the kth element.

Assuming that the self-weight is negligibly small compared to the tension forces in the membrane, the equilibrium shape is obtained by solving the following problem of minimizing $S(\mathbf{X})$ under appropriate boundary conditions:

$$\begin{aligned} &\text{Minimize} && S(\mathbf{X}) \\ &\text{subject to} && \mathbf{X}_\mathrm{L} \le \mathbf{X} \le \mathbf{X}_\mathrm{U} \end{aligned} \tag{6}$$

where $\mathbf{X}_\mathrm{L}$ and $\mathbf{X}_\mathrm{U}$ are the lower and upper bounds for $\mathbf{X}$, which are assigned for enhancing convergence properties of optimization process.

2.2 Energy minimization for pneumatic membrane

For a frame-supported pneumatic membrane structure with air pressure p, the pressure potential energy $Q(\mathbf{X})$ is given as (Coelho *et al.*, 2014b; Fischer, 1998)

$$Q(\mathbf{X}) = pV(\mathbf{X}) \tag{7}$$

where $V(\mathbf{X})$ is the volume of the air contained by the membrane structure. Let $\mathbf{X}_i^\mathrm{S} = (X_{i1}^\mathrm{S}, X_{i2}^\mathrm{S}, X_{i3}^\mathrm{S})^T$ denote the coordinate vector of node i on the curved surface, where the subscripts 1, 2, and 3 correspond to X-, Y-, and Z-components, respectively. The variable vector $\mathbf{X}$ consists of the free components of $\mathbf{X}_i^\mathrm{S}$. The coordinate vector $\bar{\mathbf{X}}_k^\mathrm{S} \in \mathbb{R}^3$ of the center of gravity of element k is defined as

$$\bar{\mathbf{X}}_k^\mathrm{S}(\mathbf{X}) = \frac{1}{3}\sum_{i \in I_k} \mathbf{X}_i^\mathrm{S} \tag{8}$$

where I_k is the set of indices of three nodes of element k.

The functions $Q(\mathbf{X})$ and $V(\mathbf{X})$ are expressed as summation of element values $Q_k^{\mathrm{e}}(\mathbf{X})$ and $V_k^{\mathrm{e}}(\mathbf{X})$, respectively. Variation of $Q(\mathbf{X})$ in the normal direction of surface is computed as

$$\begin{aligned}\delta Q(\mathbf{X}) &= \sum_{k=1}^{m} \delta Q_k^{\mathrm{e}}(\mathbf{X}) \\ &= p\sum_{k=1}^{m} \delta V_k^{\mathrm{e}}(\mathbf{X}) \\ &= p\sum_{k=1}^{m}\sum_{i\in I_k}\sum_{j=1}^{3}\left(\frac{\partial V_k^{\mathrm{e}}(\mathbf{X})}{\partial X_{ij}^{\mathrm{S}}}\delta X_{ij}^{\mathrm{S}}\right)\end{aligned} \tag{9}$$

where X_{ij}^{S} is the jth component of $\mathbf{X}_i^{\mathrm{S}}$. Let $\mathbf{n}_k(\mathbf{X}) \in \mathbb{R}^3$ denote the unit normal vector of the kth triangular element, and suppose node i belongs to element k. Then the differential coefficient of $V_k^{\mathrm{e}}(X_{ij}^{\mathrm{S}})$ with respect to X_{ij}^{S} in the normal direction of element k is written as

$$\frac{\partial V_k^{\mathrm{e}}(\mathbf{X})}{\partial X_{ij}^{\mathrm{S}}} = A_k \mathbf{n}_k(\mathbf{X})^T \frac{\partial \bar{\mathbf{X}}_k^{\mathrm{S}}(\mathbf{X})}{\partial X_{ij}^{\mathrm{S}}} \tag{10}$$

Using Eq. (10), $\delta Q(\mathbf{X})$ is further modified as

$$\begin{aligned}\delta Q(\mathbf{X}) &= p\sum_{k=1}^{m}\sum_{i\in I_k}\sum_{j=1}^{3}\left[A_k \mathbf{n}_k(\mathbf{X})^T\left(\frac{\partial \bar{\mathbf{X}}_k^{\mathrm{S}}(\mathbf{X})}{\partial X_{ij}^{\mathrm{S}}}\delta X_{ij}^{\mathrm{S}}\right)\right] \\ &= p\sum_{k=1}^{m}\sum_{i\in I_k}\sum_{j=1}^{3}\left[\frac{A_k}{3}\mathbf{n}_k(\mathbf{X})^T\left(\frac{\partial \mathbf{X}_i^{\mathrm{S}}(\mathbf{X})}{\partial X_{ij}^{\mathrm{S}}}\delta X_{ij}^{\mathrm{S}}\right)\right] \\ &= p\sum_{k=1}^{m}\sum_{i\in I_k}\sum_{j=1}^{3}\left\{\frac{A_k}{3}\mathbf{n}_k(\mathbf{X})^T\left[\begin{pmatrix}1\\0\\0\end{pmatrix}\delta X_{i1}^{\mathrm{S}} + \begin{pmatrix}0\\1\\0\end{pmatrix}\delta X_{i2}^{\mathrm{S}} + \begin{pmatrix}0\\0\\1\end{pmatrix}\delta X_{i3}^{\mathrm{S}}\right]\right\} \\ &= p\sum_{k=1}^{m}\sum_{i\in I_k}\left(\frac{A_k}{3}\mathbf{n}_k(\mathbf{X})^T \delta \mathbf{X}_i^{\mathrm{S}}\right) \\ &= p\sum_{i=1}^{n}\sum_{k\in K_i}\left(\frac{A_k}{3}\mathbf{n}_k(\mathbf{X})^T \delta \mathbf{X}_i^{\mathrm{S}}\right)\end{aligned} \tag{11}$$

where K_i is the set of elements connected to node i, and n is the number of nodes.

Using the divergence theorem, Bouzidi and Le Van (2004) derived the following expression $Q^*(\mathbf{X})$ for a membrane discretized by triangular finite elements:

$$\begin{aligned} Q^*(\mathbf{X}) &= p\int_V dV \\ &= \frac{p}{3}\int_V \operatorname{div}\mathbf{X} dV \\ &= \frac{p}{3}\int_\Gamma \mathbf{X}^T\mathbf{n}(\mathbf{X})d\Gamma \\ &= \frac{p}{3}\sum_{k=1}^{m} A_k\mathbf{n}_k(\mathbf{X})^T\bar{\mathbf{X}}_k^{\mathrm{S}}(\mathbf{X}) \end{aligned} \tag{12}$$

where Γ is the boundary of the space covered by the membrane. However, the term 1/3 in the right-hand-side of Eq. (12) is not necessary as confirmed below, because we should consider shape variation only in the normal direction of surface. Actually they did not use 1/3 in the numerical examples. Therefore, we use the following definition:

$$Q(\mathbf{X}) = p\sum_{k=1}^{m} A_k\mathbf{n}_k(\mathbf{X})^T\bar{\mathbf{X}}_k^{\mathrm{S}}(\mathbf{X}) \tag{13}$$

The equilibrium shape is obtained by minimizing the total potential energy $\Pi(\mathbf{X})$ defined as

$$\Pi(\mathbf{X}) = S(\mathbf{X}) - Q(\mathbf{X}) \tag{14}$$

Differentiation of $\Pi(\mathbf{X})$ with respect to X_{ij}^{S} leads to

$$\begin{aligned} \frac{\partial\Pi(\mathbf{X})}{\partial X_{ij}^{\mathrm{S}}} &= \sum_{k\in K_i}\left(A_k\boldsymbol{\varepsilon}_k(\mathbf{X})^T\mathbf{D}\frac{\partial\boldsymbol{\varepsilon}_k(\mathbf{X})}{\partial X_{ij}^{\mathrm{S}}}\right) - p\sum_{k\in K_i}\left(A_k\mathbf{n}_k(\mathbf{X})^T\frac{\partial\bar{\mathbf{X}}_k^{\mathrm{S}}(\mathbf{X})}{\partial X_{ij}^{\mathrm{S}}}\right) \\ &\quad - p\sum_{k\in K_i}\left(A_k\frac{\partial\mathbf{n}_k(\mathbf{X})^T}{\partial X_{ij}^{\mathrm{S}}}\bar{\mathbf{X}}_k^{\mathrm{S}}(\mathbf{X})\right) \\ &= \sum_{k\in K_i}\left(A_k\boldsymbol{\varepsilon}_k^T(\mathbf{X})\mathbf{D}\frac{\partial\boldsymbol{\varepsilon}_k(\mathbf{X})}{\partial X_{ij}^{\mathrm{S}}}\right) - \frac{p}{3}\sum_{k\in K_i}\left(A_k n_{kj}(\mathbf{X})\right) - p\sum_{k\in K_i}\left(A_k\frac{\partial\mathbf{n}_k(\mathbf{X})^T}{\partial X_{ij}^{\mathrm{e}}}\bar{\mathbf{X}}_k^{\mathrm{S}}(\mathbf{X})\right) \end{aligned} \tag{15}$$

where Eq. (8) has been used, and n_{kj} is the jth component of $\mathbf{n}_k$.

By contrast, the equilibrium equation between the air pressure and the internal force derived from strain energy is written as

$$\sum_{k\in K_i}\left(A_k\boldsymbol{\varepsilon}_k^T(\mathbf{X})\mathbf{D}\frac{\partial\boldsymbol{\varepsilon}_k(\mathbf{X})}{\partial X_{ij}^{\mathrm{S}}}\right) - \frac{p}{3}\sum_{k\in K_i}\left(A_k n_{kj}(\mathbf{X})\right) = 0\,, \quad (i=1,\ldots,n;\ j=1,2,3) \tag{16}$$

Therefore, the third term in the right-hand-side of Eq. (15), which is denoted by e_{ij} as follows, is not needed for evaluating equilibrium of membrane under air pressure:

$$e_{ij} = -p \sum_{k \in K_i} \left(A_k \frac{\partial \mathbf{n}_k(\mathbf{X})^T}{\partial X_{ij}^{\mathrm{e}}} \bar{\mathbf{X}}_k^{\mathrm{S}}(\mathbf{X}) \right) \tag{17}$$

However, it is easily seen that the additional term e_{ij} vanishes in the minimization process of $\Pi(\mathbf{X})$ as follows.

The direction of the normal vector does not change due to the variation of nodal coordinates in the direction of the plane of the element. Furthermore, the variation of normal vector due to the variation of nodes in the normal direction can be neglected within the first-order approximation. Therefore, the term $\partial \mathbf{n}_k(\mathbf{X})^T / \partial X_{ij}^{\mathrm{e}}$ vanishes, and $e_{ij} = 0$ is satisfied; accordingly, the equilibrium shape of pneumatic membrane structure can be found by solving the following problem of minimizing the energy function $\Pi(\mathbf{X})$:

$$\begin{aligned} &\text{Minimize} \quad \Pi(\mathbf{X}) \\ &\text{subject to} \quad \mathbf{X}_{\mathrm{L}} \le \mathbf{X} \le \mathbf{X}_{\mathrm{U}} \end{aligned} \tag{18}$$

3. Approximate optimization of cutting pattern

Suppose a target shape of membrane surface is given by a designer. Since the arbitrarily defined shape cannot be realized by connecting plane cutting sheets, a simple update rule of the stress parameter called *reduction stress* is proposed for approximate cutting pattern optimization. The objective here is to find the shape of cutting pattern for minimizing the variation of stresses from the *ideal target stresses*, which usually represent uniform tension state; accordingly, the target shear stress is 0. The method is based on the inverse process of generating a plane sheet from a curved surface by reducing the stress (Ohsaki and Fujiwara, 2003), and is applicable to approximate development of a surface without stress to a plane (Cui and Ohsaki, 2017, 2018).

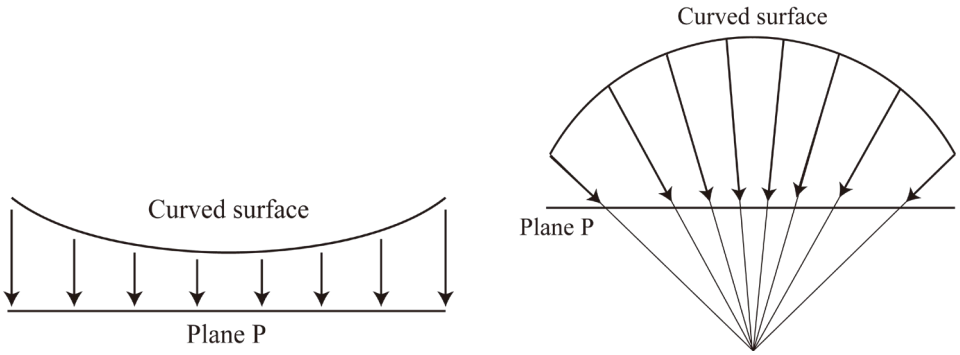

(a) (b)

Figure 2: Projection of surface to a plane; (a) small curvature, (b) large curvature.

We assign a plane P near the target surface, and project the triangular mesh onto P to generate the triangular mesh of the cutting sheet as an initial solution for optimization. If the curvature of surface is small, the plane P may be parallel to a tangent plane at the center of surface as illustrated in Fig. 2(a). By contrast, if the curvature is large as illustrated in Fig. 2(b), the surface may be projected in the direction of a point near the center of curvature.

The vector consisting of $(X^{\mathrm{P}}, Y^{\mathrm{P}})$-coordinates of the nodes of the cutting sheet on plane P is denoted by $\mathbf{X}^{\mathrm{P}} \in \mathbb{R}^{2n}$. Let $L_{k1}^{\mathrm{P}}(\mathbf{X}^{\mathrm{P}})$, $L_{k2}^{\mathrm{P}}(\mathbf{X}^{\mathrm{P}})$, and $L_{k3}^{\mathrm{P}}(\mathbf{X}^{\mathrm{P}})$ $(k=1,\ldots,m)$ denote the edge lengths of the m triangular elements on P, which are functions of $\mathbf{X}^{\mathrm{P}}$. Let L_{k1}^{0}, L_{k2}^{0}, and L_{k3}^{0} denote the unstressed lengths of three edges of element k after removing the stress from the triangular element on the curved surface. Then the following problem is solved to minimize the sum of error between the lengths of a pair of edges on the surface and on the plane:

$$\begin{aligned} &\text{Minimize} \quad F(\mathbf{X}^{\mathrm{P}}) = \sum_{k=1}^{m}\sum_{i=1}^{3} \kappa_{ki}(L_{ki}^{\mathrm{P}}(\mathbf{X}^{\mathrm{P}}) - L_{ki}^{0})^2 \\ &\text{subject to} \quad \mathbf{X}_{\mathrm{L}}^{\mathrm{P}} \le \mathbf{X}^{\mathrm{P}} \le \mathbf{X}_{\mathrm{U}}^{\mathrm{P}} \end{aligned} \tag{19}$$

where κ_{ki} is a weight parameter, and $\mathbf{X}_{\mathrm{L}}^{\mathrm{P}}$ and $\mathbf{X}_{\mathrm{U}}^{\mathrm{P}}$ are the lower and upper bounds for $\mathbf{X}^{\mathrm{P}}$. In the following examples, a large weight is given for a short edge as $\kappa_{ki} = 1/L_{ki}^{0}$ to prevent vanishing member length that may lead to reversal of a triangle on the plane.

Outline of the algorithm is illustrated in Fig. 3 and summarized as follows:

Step 1: Assign the target shape of curved surface, boundary conditions, and generate triangular meshes on the target surface. Compute the edge lengths L_{k1} L_{k2} L_{k3}

σ_{k1}^{*}, σ_{k2}^{*}, and $\tau_{k}^{*}\,(=0)$,

and initialize the reduction stress, for example, as $\hat{\sigma}_{k1}^{s}=\sigma_{k1}^{*}$, $\hat{\sigma}_{k2}^{s}=\sigma_{k2}^{*}$, and $\hat{\tau}_{k}^{s}\,(=0)$. Set the step counter as $s=0$.

Step 2: Project the triangulated surface to the plane P to find the initial values of $\mathbf{X}^{\mathrm{P}}$ for solving the optimization problem (19).

Step 3: Specify the reduction stresses $\hat{\sigma}_{k1}^{s}$, $\hat{\sigma}_{k2}^{s}$, and $\hat{\tau}_{k}^{s}\,(=0)$ in principal directions of material. Remove the stress from the triangular elements on the curved surface, and compute the unstressed edge lengths L_{k1}^{0}, L_{k2}^{0}, and L_{k3}^{0}.

Step 4: Find the nodal coordinates of the cutting sheet on plane P by solving problem (19).

Step 5: Carry out equilibrium shape analysis by solving the energy minimization problems (6) and (18), respectively, for frame-supported membrane and pneumatic membrane to find the nodal coordinates on the surface and the stresses σ_{k1}^{s}, σ_{k2}^{s}, and τ_{k}^{s} at the self-equilibrium state.

Step 6: Let $s\leftarrow s+1$, and modify the reduction stresses $\hat{\sigma}_{k1}^{s}$ and $\hat{\sigma}_{k2}^{s}$ as

$$\hat{\sigma}_{k1}^{s+1}=\hat{\sigma}_{k1}^{s}+c(\sigma_{k1}^{*}-\sigma_{k1}^{s}),\quad \hat{\sigma}_{k2}^{s+1}=\hat{\sigma}_{k2}^{s}+c(\sigma_{k2}^{*}-\sigma_{k2}^{s}),\quad \hat{\tau}_{k}^{s+1}\,(=0) \tag{20}$$

where c is the parameter for adjusting the convergence property. Also replace the target surface with the equilibrium surface obtained in Step 5.

Step 7: Go to Step 2, if the stress distribution has not converged and the number of iterative steps is less than the specified limit.

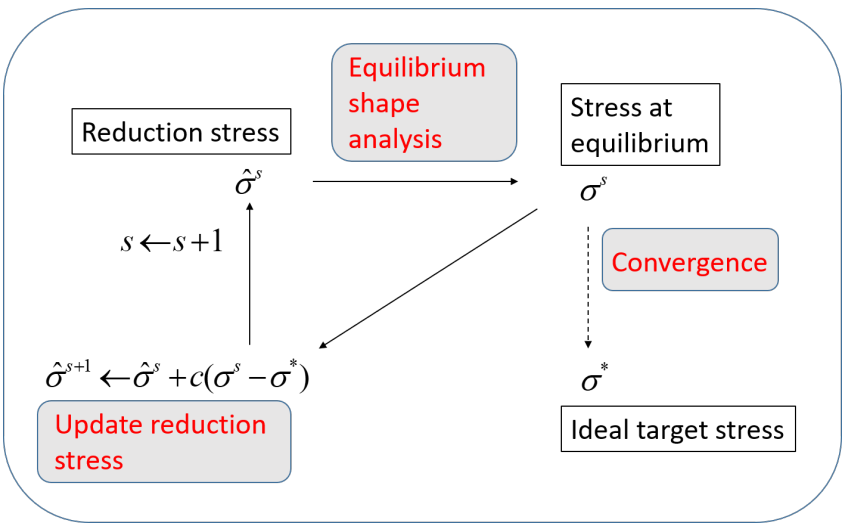

Figure 3: Outline of approximate cutting pattern optimization.

This process is illustrated using a single cable that is pin-supported at both ends. The units are omitted for brevity, and the elastic modulus E is assumed to be 1. The span length at equilibrium is $L=1.2$. The problem is to find the unstressed length of the cable so that the stress after connecting the both ends to the supports becomes 0.1. In order to follow the process for membrane structures, for which the shape of a triangular element at equilibrium is not known, the initial guess for the length at equilibrium is assumed to be $\bar{L}=1.0$, although it is known as 1.2. Parameter c is equal to 1.0. The process is listed as follows and is illustrated in Fig. 4:

Step 1. Assign the reduction stress $\hat{\sigma}^1$ equal to the ideal target stress as $\hat{\sigma}^1=\sigma^*=0.1$.
Compute the unstressed length as $L_0=\bar{L}\times(1.0-0.1)=1.0\times(1.0-0.1)=0.9$.

Compute the stress at equilibrium as $\sigma^1=(L-L_0)/L_0=(1.2-0.9)/0.9=0.33$.

Step 2. Update the reduction stress as

$\hat{\sigma}^2=\hat{\sigma}^1+c(\sigma^*-\sigma^1)=0.1+1.0\times(0.1-0.33)=-0.13$.

Compute the unstressed length as $L_0=\bar{L}\times(1.0+0.13)=1.0\times(1.0+0.13)=1.13$.

Compute the stress at equilibrium as $\sigma^2=(L-L_0)/L_0=(1.2-1.13)/1.13=0.06$.

Step 3. Update the reduction stress as

$\hat{\sigma}^3=\hat{\sigma}^2+c(\sigma^*-\sigma^2)=-0.13+1.0\times(0.1-0.06)=-0.09$.

Compute the unstressed length as $L_0=\bar{L}\times(1.0+0.09)=1.0\times(1.0+0.09)=1.09$.

Compute the stress at equilibrium as $\sigma^3=(L-L_0)/L_0=(1.2-1.09)/1.09=0.10$.

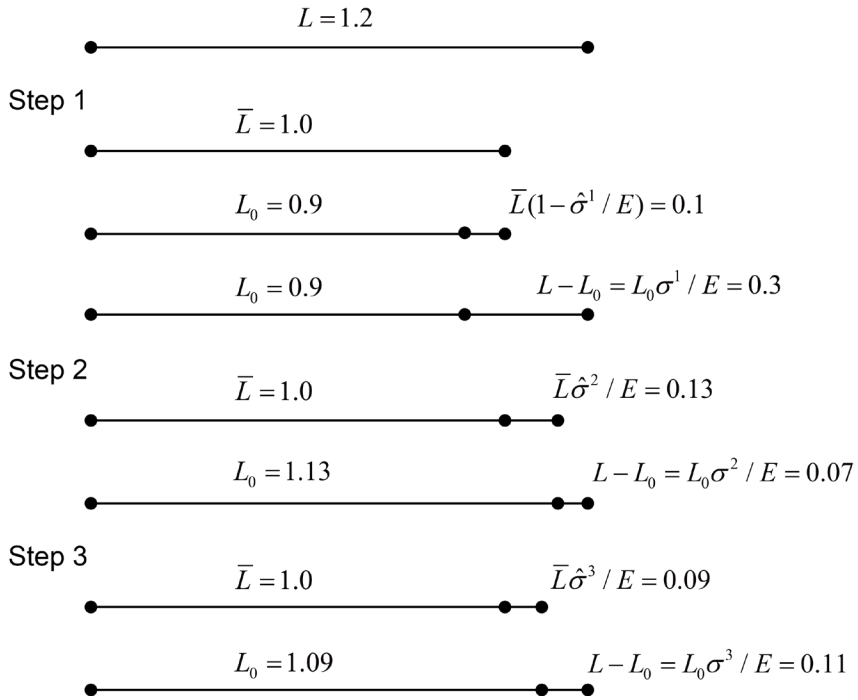

Figure 4: Illustration of proposed procedure using a cable model.

This way, the correct unstressed length 1.09 and the stress at equilibrium 0.1 have been found with three iterations.

As seen from this result of a cable, initial guess of the length $\bar{L}$ does not have any effect on the final shape. Accordingly, the reduction stress is regarded as a controlling parameter that is not related to the final stress at equilibrium. Therefore, for a membrane structure, the accuracy of the projected shape on the plane is not very important.

4. Analysis of ETFE film

ETFE film is usually modeled as an elasto-plastic material with von Mises yield criterion (Yoshino and Kato, 2016; Coelho *et al*., 2015). However, the method of cutting pattern design described in Sec. 3 is applicable only to elastic membrane material. Furthermore, only monotonic loading is considered in the process of increasing the pressure to reach the equilibrium shape. Therefore, in this section, an approximation method is presented for ETFE film for a pneumatic membrane structure using nonlinear isotropic elastic material model.

The relation between stress and strain of an elasto-plastic material in uniaxial tension is often modeled as bilinear relation, which is identified by experiments as shown in Fig. 5, where σ^{Y} ε^{Y}

may be regarded as a relation between equivalent stress and strain. Since the stiffness after yielding is smaller than the initial elastic stiffness, almost uniform stress distribution can be expected, if the target stress σ^* is larger than σ^{Y}.

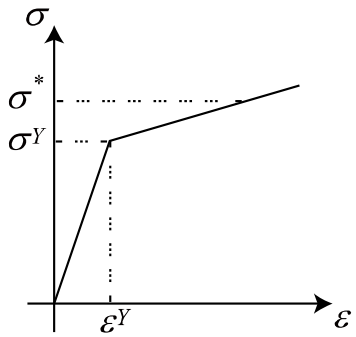

Figure 5: Relation between equivalent stress σ and equivalent strain ε of ETFE sheet under uniaxial tension.

Let E, H and $\mathbf{D}_1 \in \mathbb{R}^{3\times3}$ denote elastic modulus, hardening coefficient, and isotropic elastic constitutive matrix, respectively. To model the stress-strain relation as nonlinear elastic, the constitutive matrix after yielding is given as

$$\mathbf{D}_2 = \frac{H}{E}\mathbf{D}_1 \tag{21}$$

In the process of energy minimization for finding the self-equilibrium shape, the trial stress vector $\tilde{\boldsymbol{\sigma}} = (\tilde{\sigma}_x, \tilde{\sigma}_y, \tilde{\tau})^T$ with respect to the local coordinates (x, y) of element is first calculated as follows from the strain vector $\boldsymbol{\varepsilon} = (\varepsilon_x, \varepsilon_y, \gamma)^T$ with respect to the (x, y)-coordinates, which is calculated from the nodal coordinates on the surface using Eq. (5):

$$\tilde{\boldsymbol{\sigma}} = \mathbf{D}_1\boldsymbol{\varepsilon} \tag{22}$$

Then, the equivalent stress $\tilde{\sigma}_{\mathrm{eq}}$ corresponding to $\tilde{\boldsymbol{\sigma}}$ is obtained from

$$\tilde{\sigma}_{\mathrm{eq}} = \sqrt{(\tilde{\sigma}_x)^2 - \tilde{\sigma}_x\tilde{\sigma}_y + (\tilde{\sigma}_y)^2 + 3\tilde{\tau}^2} \tag{23}$$

From the ratio of the yield stress σ^{Y} to $\tilde{\sigma}_{\mathrm{eq}}$, the strain vector at the yield point $\boldsymbol{\varepsilon}^{\mathrm{Y}}$ is computed as

$$\boldsymbol{\varepsilon}^{\mathrm{Y}} = \frac{\sigma^{\mathrm{Y}}}{\tilde{\sigma}_{\mathrm{eq}}}\boldsymbol{\varepsilon} \tag{24}$$

Therefore, the stress vector is obtained using E, H, $\mathbf{D}_1$, and $\boldsymbol{\varepsilon}^{\mathrm{Y}}$ as

$$\begin{aligned}\boldsymbol{\sigma} &= \mathbf{D}_1\boldsymbol{\varepsilon}^{\mathrm{Y}} + \mathbf{D}_2(\boldsymbol{\varepsilon}-\boldsymbol{\varepsilon}^{\mathrm{Y}}) \\ &= \left(1-\frac{H}{E}\right)\mathbf{D}_1\boldsymbol{\varepsilon}^{\mathrm{Y}} + \frac{H}{E}\mathbf{D}_1\boldsymbol{\varepsilon}\end{aligned} \tag{25}$$

and the strain energy density S is computed from

$$S = \left(1-\frac{H}{E}\right)\boldsymbol{\varepsilon}^T\mathbf{D}_1\boldsymbol{\varepsilon}^{\mathrm{Y}} + \frac{H}{2E}\boldsymbol{\varepsilon}^T\mathbf{D}_1\boldsymbol{\varepsilon} \tag{26}$$

Although the stiffness after yielding depends on the stress ratio between σ_x and σ_y, we assume the ideal state satisfying $\sigma_x = \sigma_y$ for which the relation between the equivalent stress and equivalent strain is obtained by experiment. The vector consisting of the yiels stress is denoted by $\boldsymbol{\sigma}^{\mathrm{Y}} = (\sigma^{\mathrm{Y}}, \sigma^{\mathrm{Y}}, 0)^T$. Since we consider a monotonic loading process, the equilibrium shape of an air-pressured ETFE film can be obtained by minimizing $\Pi(\mathbf{X}) = S(\mathbf{X}) - Q(\mathbf{X})$ with the following definition of $S(\mathbf{X})$:

$$S(\mathbf{X}) = \frac{1}{2}\sum_{k=1}^{m} A_k\left[\boldsymbol{\varepsilon}_k^{\mathrm{Y}T}\boldsymbol{\sigma}^{\mathrm{Y}} + \left(\boldsymbol{\varepsilon}_k - \boldsymbol{\varepsilon}_k^{\mathrm{Y}}\right)^T\left(\boldsymbol{\sigma}_k + \boldsymbol{\sigma}^{\mathrm{Y}}\right)\right] \tag{27}$$

5. Numerical examples

The proposed algorithm of approximate cutting pattern optimization is applied to a frame-supported PVC membrane (PVC-coated polyester fabric) and an air-pressured ETFE film. The optimization problems are solved using sequential quadratic programming (Long *et al*., 2019) implemented in SNOPT Ver. 7 (Gill *et al*., 2002), where the sensitivity coefficients are computed analytically. Details are not shown here, because the sensitivity equations are derived by simply differentiating the governing equations; see, e.g., Wang *et al*. (1992) and Choi and Kim (2005) for details. Triangular mesh is generated using the Delaunay triangulation library available in scipy.spatial package (SciPy, 2019). The size of structural model is indicated by the parameter W and the aspect ratio, because the stress values at equilibrium do not depend on the size of the structure, when it is uniformly scaled.

5.1 Model 1: Frame-supported PVC membrane

Consider a frame-supported membrane with hyperbolic paraboloid surface (Model 1) as shown in Fig. 5. Proportion of the model is $W_1 = 1.0W$, $W_2 = 1.3W$, and $H = 0.2W$. The material property is assumed to be orthotropic elastic as described in Sec. 2.1. Elastic moduli in warp and weft directions are $E_x = 2.43 \times 10^2$ kN/m and $E_y = 2.27 \times 10^2$ kN/m, respectively. The shear modulus G is 24.2 kN/m, and Poisson's ratio is $\nu_{xy} = 0.51$. These material parameters are obtained from bi-axial and shear tests according to the testing methods of Membrane Structures Association of Japan (Membrane Struct. Assoc. Japan, 1993, 1995). The membrane is divided into two cutting sheets along the dashed line shown in Fig. 7(a). The total numbers of nodes and elements are 160 and 240, respectively. The curved surface is projected to a plane that is parallel to the global XY-plane. A sufficiently large range is given for the coordinate variables in Eq. (6); the lower and upper bounds are $-10W$ and $20W$, respectively. The lower and upper bounds for the coordinates on the plane in Eq. (19) are $-5W$ and $20W$, respectively. Note that these values do not have any effect on the solutions if the ranges of variables are sufficiently large.

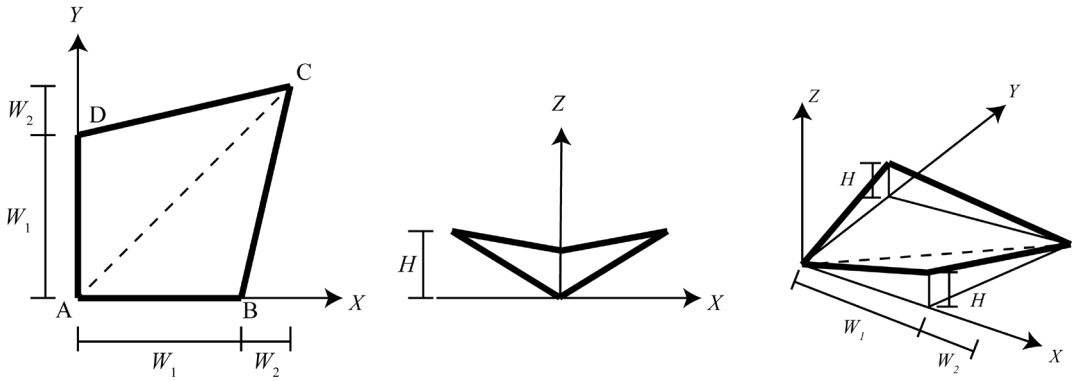

(a) (b) (c)

Figure 6: A frame-supported membrane with hyperbolic paraboloid surface (Model 1); (a) plan, (b) elevation, (c) diagonal view.

The target stress is 3.0 kN/m in both warp and weft directions, which are X and Y directions, respectively, of the global coordinates of the cutting sheet indicated in Fig. 7(b). We first carried out the proposed process with different values of parameter c for adjusting the convergence property in Eq. (20). As seen in Fig. 8, a small value of c leads to gradual convergence, while a large value results in rapid convergence after a large error in the first few steps. Based on this result, the parameter value $c = 0.5$ is chosen for Model 1.

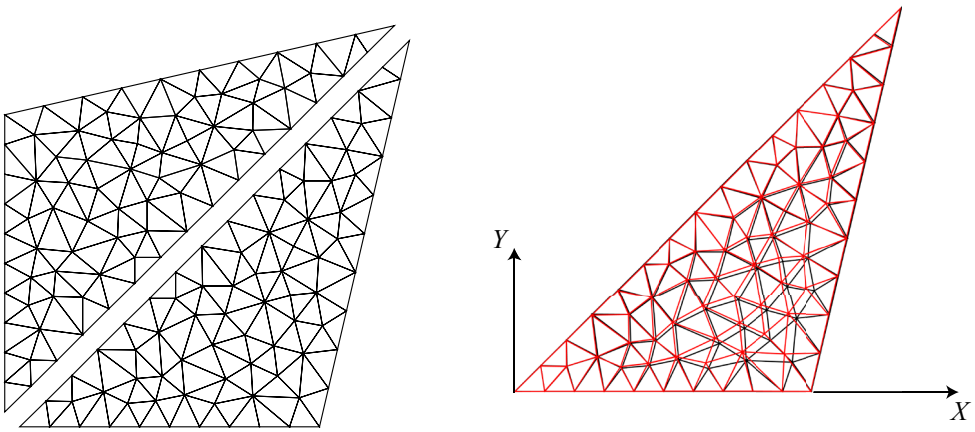

(a) (b)

Figure 7: Cutting sheets of Model 1: (a) triangular mesh, (b) triangular mesh projected to *XY*-plane before optimization (black) and cutting sheet after optimization (red).

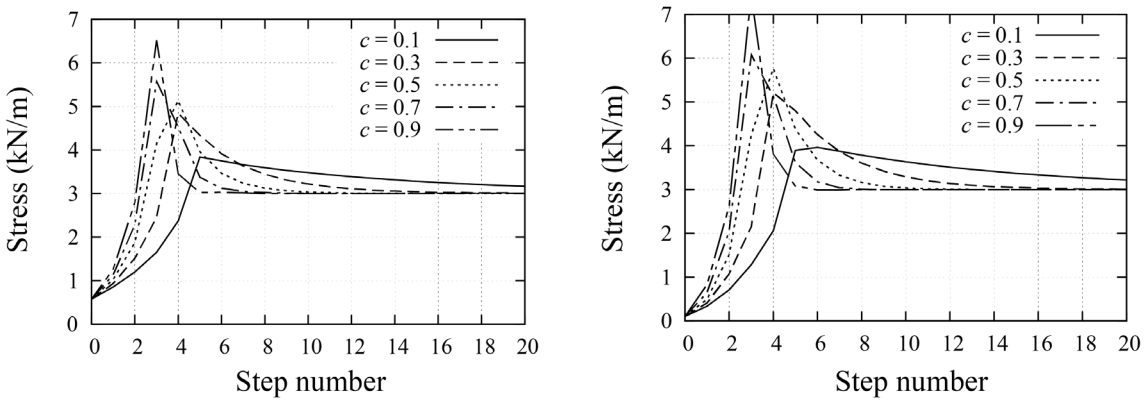

(a) (b)

Figure 8: Variation of average stresses for different values of parameter c for adjusting the convergence property in Eq. (20); (a) warp (X) direction, (b) weft (Y) direction.

The histories of average, maximum, minimum values, and standard deviation of stress are listed in Table 1, where X and Y denote the directions of warp and weft, respectively. As seen from the table, the minimum value increases from a negative value to a positive value. The average value gradually converges to the target value. The minimum and maximum stresses are close enough to the target value at the 10th step. The cutting pattern at the 20th step is shown in Fig. 7(b). Note that the cutting pattern is close to the triangular plan of the half part of surface, which means that the area of cutting sheet is smaller than the surface area. The stress distribution at the

20th step is shown in Fig. 9. As seen from the figure, the stresses in warp and weft directions are almost uniform except in the area near corners. It is notable that almost uniform stress distribution can be achieved using only two cutting sheets.

Table 1: Histories of average, maximum, minimum values, and standard deviation of stress (kN/m) of Model 1.

	Step 0		Step 5		Step 10		Step 15		Step 20	
Direction	*X*	*Y*	*X*	*Y*	*X*	*Y*	*X*	*Y*	*X*	*Y*
Average	0.577	0.102	3.964	4.378	3.034	3.036	3.003	3.002	3.002	3.004
Max.	3.320	2.811	7.468	5.513	3.312	3.093	3.222	3.072	3.237	3.072
Min.	−16.619	−2.680	3.286	3.220	2.960	2.987	2.931	2.951	2.931	2.952
Std. Dev.	2.202	0.621	0.784	0.624	0.063	0.018	0.053	0.019	0.053	0.019

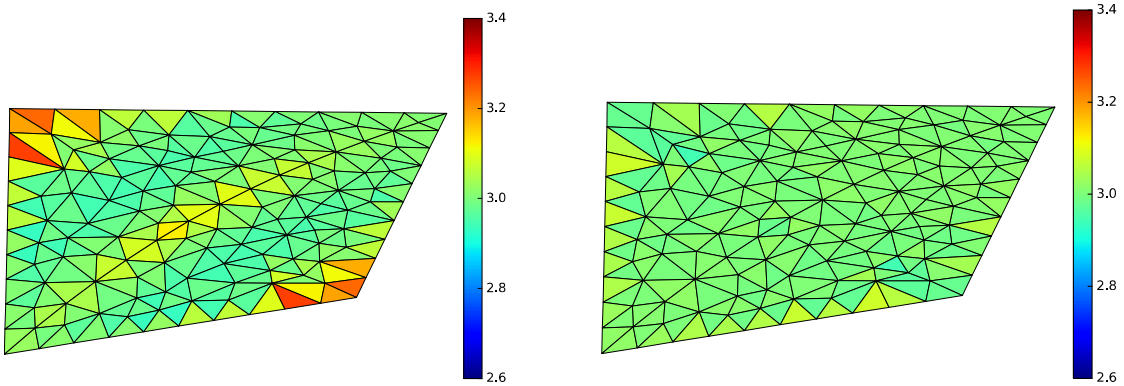

(a) (b)

Figure 9: Stress distribution (kN/m) after 20 steps of iteration: (a) warp direction, (b) weft direction.

5.6 Model 2: Air-pressured ETFE film

Consider an air-pressured ETFE cushion, which has a square plan as shown in Fig. 10, where the ratio of H to W of the circular arch along the boundary is 0.058. The ETFE cushion is divided into two cutting sheets along the dashed line shown in Fig. 10(a). The material property is isotropic nonlinear elastic as described in Sec. 4. Thickness is 200 μm, elastic modulus is 1.60×10^2 kN/m, hardening coefficient is 10.4 kN/m, elastic shear modulus is 55.2 kN/m, shear modulus after yielding is 3.60 kN/m, Poisson's ratio is 0.45, and the stress and strain at yielding is 3.2 kN/m and 0.02, respectively. The specified air pressure is $3.0/W$

$2\times 4.0/(3.0/W)=2.667W$, if the surface is spherical. The curved surface is projected in the direction of the center of curvature of the surface as illustrated in Fig. 2(b). The lower and upper bounds for the coordinates in Eq. (18) are $-3.333W$ and $6.667W$, respectively. The lower and upper bounds for the coordinates on the plane in Eq. (19) are $-1.667W$ and $6.667W$, respectively.

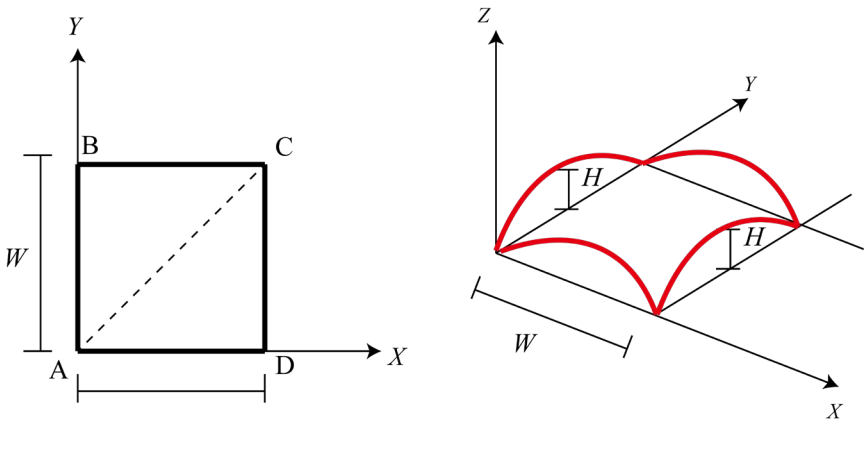

(a) (b)

Figure 10: Air-supported ETFE sheet (Model 2); (a) plane, (b) diagonal view.

Table 2: Histories of average, maximum, minimum values, and standard deviation of stress (kN/m) of Model 2.

	Step 0		Step 2		Step 4		Step 7		Step 10	
Direction	*X*	*Y*	*X*	*Y*	*X*	*Y*	*X*	*Y*	*X*	*Y*
Average	4.589	4.591	5.015	5.025	5.056	5.052	4.024	4.023	4.063	4.063
Max.	5.175	5.151	6.635	6.599	7.320	7.221	4.526	4.609	4.652	4.795
Min.	–1.155	–1.110	3.025	3.237	3.250	3.568	2.969	3.176	2.744	2.964
Std. Dev.	0.633	0.624	0.649	0.644	0.806	0.814	0.268	0.272	0.290	0.301

We carried out several trials for determining the value of c in Eq. (20). Since the stiffness of the ETFE is discontinuous due to yielding, a small value 0.05 has been chosen for c. The histories of average, maximum, minimum values and standard deviation of stress are listed in Table 2, where X and Y denote the directions in X- and Y-directions on the global coordinates of the cutting sheet as indicated in Fig. 11. The cutting patterns before and after optimization are shown in Fig. 11, and

stress distributions in *X*- and *Y*-directions after 10 steps are shown in Figs. 12(a) and (b), respectively. It is seen from these results that the cutting pattern is significantly different from the triangular shape, because the ratio of maximum height to the span *W* has a moderately large value 0.2204. It is notable also for this model that almost uniform stress distribution can be achieved using only two cutting sheets.

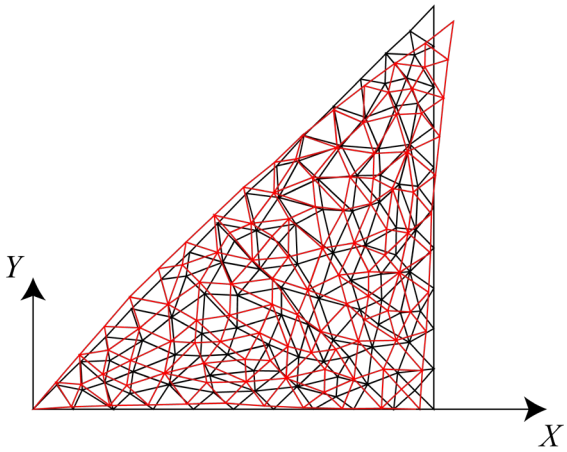

Figure 11: Cutting sheet of Model 2: triangular mesh projected to *XY*-plane before optimization (black) and cutting sheet after optimization (red).

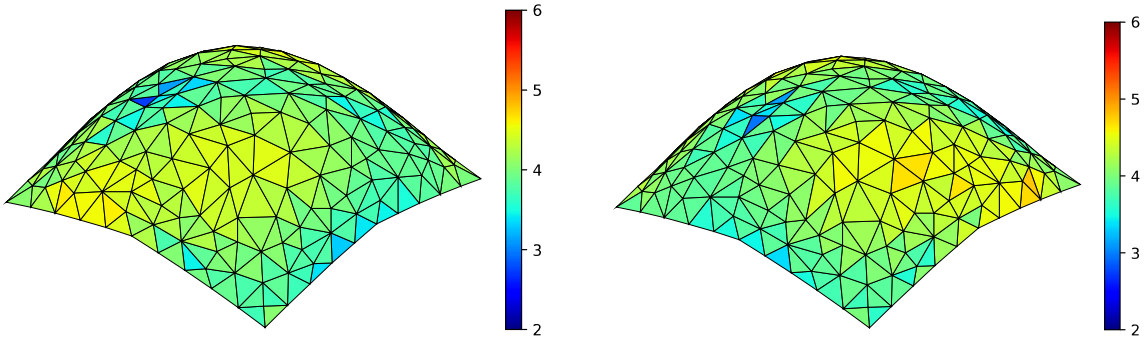

(a) (b)

Figure 12: Stress distribution (kN/m) after 10 steps of iteration; (a) *X*-direction, (b) *Y*-direction.

6. Conclusions

An approximate method has been presented for cutting pattern optimization of membrane structures. The method is based on an inverse process of removing the specified target stress from the self-equilibrium state of curved surface. The surface and cutting sheets are divided into

triangular elements with uniform plane stress, and the material properties are assumed to be orthotropic elastic for the PVC coated (polyester) fabric and bilinear nonlinear isotropic elastic for the ETFE film.

The approximate plane cutting pattern for the curved surface with specified target stress is obtained by removing the stresses of triangular elements and minimizing the norm of errors of the edge lengths from those of the triangular elements on a plane. By adjusting the stress parameter called reduction stress, an approximate optimal cutting pattern can be obtained after several iterations of cutting pattern generation and equilibrium shape analysis, which is formulated as an optimization problem of minimizing the strain energy under forced displacements at the boundary of a frame supported membrane structure. Note that the reduction stress is regarded as a parameter for controlling the shape of cutting pattern; i.e., it does not represent the ideal target stress.

The equilibrium shape of a pneumatic membrane structure can also be obtained by minimizing the total potential energy including the work done by the air pressure. A formulation of pressure potential is obtained based on the shape variation in the normal direction of the surface. The material property of an ETFE sheet can be modeled as bilinear nonlinear elastic in the process of monotonically increasing the pressure to form the equilibrium shape. It has been shown in the numerical examples that almost uniform stress distribution is achieved for a frame-supported PVC membrane and an ETFE film subjected to air pressure using only two triangular cutting sheets.

References

[1] Adriaenssens, S., Block, P., Veenendaal, D., Williams, C. (Eds.). Shell Structures in Architecture. Routledge (2014)

[2] Azariadis, P.N., Aspragathos, N.A.: Geodesic curvature preservation in surface flattening through constrained global optimization. Computer-Aided Design. **33**, 581–591 (2001)

[3] Barnes, M.R.: Form-finding and analysis of prestressed nets and membranes. Comp. Struct. **30**(3), 685–695 (1988)

[4] Bathe, K.-J.: Finite Element Procedures. Prentice-Hall (1996)

[5] Bletzinger, K.-U., Wünchmer, R., Daoud, F., Camprubi, N.: Computational methods for form finding and optimization of shells and membranes. Comput. Meth. Appl. Mech. Eng. **194**, 3438–3452 (2005)

[6] Bouzidi, R., Le Van, A.: Numerical solution of hyperelastic membranes by energy minimization. Comp. Struct. **82**, 1961–1969 (2004)

[7] Bown, A, Wakefield, D.: Inflatable membrane structures in architecture and aerospace: Some recent projects. J. Int. Assoc. Shell and Spatial Struct. **56**(1), 5–16 (2015)

[8] Choi, K.K., Kim, N.-H.: Structural Sensitivity Analysis and Optimization 1: Linear Systems. Springer (2005)

[9] Coelho, M., Roehl, D., Bletzinger, K.-U.: Numerical simulation of burst-test of an ETFE membrane. Proc. IASS Symposium, Brasilia, Int. Assoc. Shell and Spatial Struct. Paper No. 293 (2014a)

[10] Coelho, M., Roehl, D., Bletzinger, K.-U.: Numerical and analytical solutions with finite strain for circular inflated membranes considering pressure-volume coupling. Int. J. Mech. Sci. **82**, 122–130 (2014b)

[11] Cui, J., Ohsaki, M.: An optimization method for generating self-equilibrium shape of curved surface from developable surface. Proc. IASS Symposium 2017, Hamburg, Germany, Int. Assoc. Shell and Spatial Struct. Paper No. 9576 (2017)

[12] Cui, J., Ohsaki, M.: Shape design of curved surface of membrane structure using developable surface. J. Int. Assoc. Shell and Spatial Struct. **59**(3), 199–214 (2018)

[13] Daxini, S.D., Prajapati, J.M.: Structural shape optimization with meshless method and swarm-intelligence based optimization. Int. J. Mechanic and Materials in Design. Published online (2019)

[14] Dinh, T.D., Rezael, A., Puystiens, S., van Craenenbroeck, M., Carbonez, K., de Laet, L., Mollaert, M., van Hemelrick, D., van Paepegem, W.: A study of tension fabric membrane structures under in-plane loading: Nonlinear finite element analysis and validation. Composite Structures. **128**, 10–20 (2015)

[15] Dinh, T.D., Razaei, A., Punurai, W., de Laet, L., Molleart, M., van Hemelrijck, D., van Paepegem, W.: A shape optimization approach to integrated design and nonlinear analysis of tensioned fabric membrane structures with boundary cables. Int. J. Solids Struct. **83**, 114–125 (2016)

[16] Fischer, D., Configuration dependent pressure potentials. J. Elasticity. **19**, 77–84 (1998)

[17] Gill, P.E., Murray, W., Saunders, M.A.: SNOPT: An SQP algorithm for large-scale constrained optimization. SIAM J. Opt. **12**, 979–1006 (2002)

[18] Gosling, P.D., Lewis, W.J.: Optimal structural membranes: I. Formulation of a curved quadrilateral element for surface definition. Comp. Struct. **61**(5), 871–883 (1996)

[19] Hu, J., Gao, C., He, S., Chen, W., Li, Y., Zhao, B., Shi, T., Yang, D.: Effects of on-axis and off-axis tension on uniaxial mechanical properties of plain woven fabrics for inflated structures. Composite Structures. **171**, 92–99 (2017)

[20] Kim, J.-Y., Lee, J.-B.: A new technique for optimum cutting patterns generation of membrane structures. Eng. Struct. **24**, 745–756 (2002)

[21] Long, K., Wang, X., Du, Y.: Robust topology optimization formulation including local failure and load uncertainty using sequential quadratic programming. Int. J. Mechanic and Materials in Design. **15**, 317–332 (2019)

[22] Luo, Y., Xing, J., Niu, Y. Li, M., Kang, Z.: Wrinkle-free design of thin membrane structures using stress-based topology optimization. J. Mech. Phys. Solids. **102**, 277–293 (2017)

[23] Membrane Structures Association of Japan.: Testing Method for In-plane Shear Properties of Membrane Materials. MSAJ/M-01-1993. (1993) (in Japanese)

[24] Membrane Structures Association of Japan.: Testing Method for Elastic Constants of Membrane Materials. MSAJ/M-02-1995 (1995) (in Japanese)

[25] Morozov, E.V., Lopatin, A.V.: Analysis and design of the flexible composite membrane stretched on the spacecraft solar frame. Composite Structures **94**, 3106–3114 (2012)

[26] Mosler, J.: A novel variational algorithmic formulation for wrinkling at finite strains based on energy minimization: Application to mesh adaptation. Comp. Meth. Appl. Mech. Engrg. **197**, 1131–1146 (2008)

[27] Ohsaki, M., Fujiwara, J.: Developability conditions for prestress optimization of a curved surface. Comp. Meth. Appl. Mech. Engng. **192**, 77–94 (2003)

[28] Ohsaki, M., Saburi, S., Takeda, F.: Approximate method for cutting pattern optimization of membrane structures. Proc. IASS Symposium 2017, Hamburg, Germany, Int. Assoc. Shell and Spatial Struct. Paper No. 9503 (2017)

[29] Ohsaki, M., Uetani, K.: Shape-stress trade-off design of membrane structures for specified sequence of boundary shapes. Comp. Meth. Appl. Mech. Engng. **182**, 73–88 (2000)

[30] Pargana, J.B., Lloyd-Smith, D., Izzuddin, B.A.: Advanced material model for coated fabric used in tensioned fabric structures. Eng. Struct. **29**, 1323–1336 (2007)

[31] Philipp, B., Dieringer, F., Wüchner, R., Bletzinger, K.-U.: Form-finding and structural analysis for the design of hybrid structures. J. Int. Assoc. Shell and Spatial Struct. **56**(1), 17–25 (2015)

[32] Punurai, W., Tongpool, W., Morales, J.H.: Implementation of genetic algorithm for optimum cutting pattern generation of wrinkle free finishing membrane structures. Finite Elements in Analysis and Design. **58**, 84–90 (2012)

[33] SciPy. https://docs.scipy.org/doc/scipy/reference/spatial.html (accessed on June 11,2019)

[34] Uetani, K., Mitsuda, E., Ohsaki, M.: Cutting pattern optimization of frame-supported membranes considering boundary shape and stress ratio as design parameters. J. Struct. Constr. Eng., Architectural Institute of Japan. **66**(540), 73–78 (2001) (in Japanese)

[35] Wang, B.P., Babu, D., Nambiar, R.V., Lawrence, K.L.: Shape sensitivity analysis using closed-form stiffness matrix for hierarchic triangular elements. Comp. Struct. **43**(1), 69–75 (1992)

[36] Wang, C.C.L., Smith, S.S.-F., Yuen, M.M.F.: Surface flattening based on energy model. Computer-Aided Design. **34**, 823–833 (2002)

[37] Wang, Q., Pejhan, K., Telichev, I., Wu, C.Q.: Extensions of the U* theory for applications on orthotropic composites and nonlinear elastic materials. Int. J. Mechanic and Materials in Design. **13**, 469–480 (2017)

[38] Xing, J., Luo, Y., Zhan, J., Kang, Z.: Global shape optimization of fixtures to suppress wrinkles in large-displacement membrane structures. Int. J. Solids Struct. **144**–**145**, 301–312 (2018)

[39] Yoshino, T., Kato, S.: Viscous characteristics of ETFE film sheet under equal biaxial tensions. Procedia Eng. **155**, 442–451 (2016)

[40] Zhao, T., Ramos Jr., A.S., Paulino, G.H.: Material nonlinear topology optimization considering the von Mises criterion through an asymptotic approach: Max strain energy and max load factor formulations. Int. J. Numer. Meth. Engng. **118**(13), 804–828 (2019)